

# DVG-Diffusion: Dual-View Guided Diffusion Model for CT Reconstruction from X-Rays

Xing Xie<sup>\*</sup>, Jiawei Liu<sup>\*</sup>, Huijie Fan, Zhi Han, Yandong Tang, and Liangqiong Qu

**Abstract**—Directly reconstructing 3D CT volume from few-view 2D X-rays using an end-to-end deep learning network is a challenging task, as X-ray images are merely projection views of the 3D CT volume. In this work, we facilitate complex 2D X-ray image to 3D CT mapping by incorporating new view synthesis, and reduce the learning difficulty through view-guided feature alignment. Specifically, we propose a dual-view guided diffusion model (DVG-Diffusion), which couples a real input X-ray view and a synthesized new X-ray view to jointly guide CT reconstruction. First, a novel view parameter-guided encoder captures features from X-rays that are spatially aligned with CT. Next, we concatenate the extracted dual-view features as conditions for the latent diffusion model to learn and refine the CT latent representation. Finally, the CT latent representation is decoded into a CT volume in pixel space. By incorporating view parameter guided encoding and dual-view guided CT reconstruction, our DVG-Diffusion can achieve an effective balance between high fidelity and perceptual quality for CT reconstruction. Experimental results demonstrate our method outperforms state-of-the-art methods. Based on experiments, the comprehensive analysis and discussions for views and reconstruction are also presented.

**Index Terms**—Diffusion model, CT Reconstruction, X-rays, 2D-to-3D

## I. INTRODUCTION

COMPUTED tomography (CT) is a widely used imaging technique in medical diagnosis, and can provide detailed internal images of various body parts [1]. However, the scanning process of CT exposes patients to large amounts of ionizing radiation [2], and the high cost of CT scanners also limits their widespread availability in some clinics and developing countries. Additionally, CT requires patients to be scanned in a lying position, which is unsuitable for some special patients and diseases, such as spinal disorders [3]. In contrast, X-ray imaging is one of the most common examinations in hospitals, especially in clinics, offering advantages such as low radiation,

affordability and wide availability for patients. However, X-ray imaging provides only limited 2D information without 3D view, which limits its availability for clinical diagnosis, especially for early diagnosis of diseases.

In recent years, AI-driven medical image synthesis has achieved remarkable successes [4]–[10], including CT reconstruction from a single-planar or biplanar X-rays [11]–[17]. Ying *et al.* [13] pioneered the X2CT-GAN, demonstrating that generative adversarial network (GAN) can be used to learn the X-rays-to-CT mapping in an end-to-end manner. Since then, various subsequent techniques have been further developed to improve CT reconstruction, such as incorporating depth information [14], multitask learning [17], and shape estimation schemes [18]. These methods enhance reconstruction performance with estimated depth, segmentation map, or other information. However, they rely heavily on the accuracy of the estimated information, which leads to performance degradation when the acquired prior is inaccurate, affecting their applications.

To avoid reliance on estimation information, some researchers attempt to directly learn the mapping between 2D X-ray images and 3D CT volume. They designed multichannel residual block [11], feature attention module [3] and transformer module [19], achieving promising reconstruction results. However, these direct X-rays-to-CT mapping methods are inherently challenged by the lack of one-to-one correspondence, as the X-ray image is only a projection view of the 3D CT volume, which compromises reconstruction accuracy. In [13], [14], Ying *et al.* highlighted that providing more real X-ray views as input can significantly enhance CT reconstruction, as these extra views offer complementary information to reduce the learning ambiguity. Despite these findings, acquiring multiple X-ray views for a single patient is often impractical due to constraints such as increased time costs, patient discomfort, and the need for efficient medical workflows. This practical barrier prompts a critical, yet underexplored, question: *Instead of relying solely on the limited available X-ray views for CT reconstruction, can the synthesis of additional X-ray views and their joint utilization with the original input view facilitate the CT reconstruction process?*

To answer the above question, we propose a novel approach called the Dual View Guided Diffusion model (DVG-Diffusion), which couples real input X-ray views with a synthesized new X-ray view to jointly guide CT reconstruction and refinement. The core of our DVG-Diffusion lies in a novel View Parameter Guided Encoder (VPGE) that back-projects the X-rays into a 3D latent space aligned as closely as possible with the CT latent space. As shown in Fig. 1, in

This work is supported by the National Natural Science Foundation of China (62306253, U23A20343, U20A20200, 61873259), Guangdong Natural Science Fund-General Programme (2024A1515010233), and the Youth Innovation Promotion Association of Chinese Academy of Sciences(Y202051). (Xing Xie and Jiawei Liu contributed equally to this work.) (Corresponding authors: Liangqiong Qu; Zhi Han)

X. Xie and J. Liu are with State Key Laboratory of Robotics, Shenyang Institute of Automation, Chinese Academy of Sciences, Shenyang, 110016, China; University of Chinese Academy of Sciences, Beijing, 100049, China (email: (xiexing.liujiawei)@sia.cn).

H. Fan, Z. Han and Y. Tang are with State Key Laboratory of Robotics, Shenyang Institute of Automation, Chinese Academy of Sciences, Shenyang, 110016, China; (email: {fanhuijie,hanzhi,ytang}@sia.cn).

L. Qu is with the Department of Statistics and Actuarial Science and the Institute of Data Science, The University of Hong Kong, Hong Kong, 999077 (e-mail: liangqqu@hku.hk).

DVG-Diffusion, a new X-ray view is first synthesized from the given X-rays (Fig. 1(b)). The VPGE module generates dual-view features by extracting features from both the synthetic X-ray view and the input X-ray view. These dual-view features serve as conditions for the latent diffusion model to learn and refine the CT latent representation, which is then decoded back into pixel space for CT reconstruction. Overall, we utilize the additional synthesized X-ray view and leverage the VPGE module to establish spatially coherent representations between X-rays and CT modalities. Generation in aligned latent space ensures the perceptual quality, while additional view guidance enhances the fidelity. By this way, our DVG-Diffusion model achieves a remarkable balance between high fidelity and high perceptual quality for CT reconstruction.

The main contributions are summarized below:

- We propose a novel dual-view guided diffusion model (DVG-Diffusion), marking the first instance of intergrating the additional view of synthesized new X-rays into CT reconstruction. This synthetic view provides complementary information, thereby enhancing the reconstruction performance.
- We propose a view parameter guided encoder (VPGE) that back-projects the X-ray into a 3D latent space that aligns more readily with the CT latent space. This approach transforms the original intricate 2D-to-3D pixel space mapping into a more feasible 3D-to-3D latent space mapping.
- Experimental results show that our method achieves state-of-the-art results, realizing the effective reconstruction of the 3D structure. Our experiments also provide valuable insights about the relationship between views and reconstruction.

## II. RELATED WORK

The conversion from 2D images to 3D volumes is a challenging task, as it involves recovering volumetric information from a limited number of projections. We review the methods for 3D reconstruction in CT and natural images, respectively.

### A. 3D CT Reconstruction from 2D X-Rays

Currently, the most promising solution for learning X-ray-to-CT mappings is deep learning. Initial work by Henzler *et al.* [20] proposed a 2D deep neural network (2DCNN) for reconstructing 3D volumes from 2D X-ray images. Shen *et al.* [15] improved 2DCNN by using patient-specific CT images for training and introducing a dimensional change module to facilitate 2D-3D mapping. However, these CNN-based methods rely on pixel-level constraints, potentially leading to overly smooth CT images. To address this issue, Ying *et al.* [13] employed adversarial loss in their X2CT-GAN model, enhancing the perceptual details of reconstructed CT images. Since then, several other GAN-based models were developed [11], [14], [19]. However, the samples generated by GAN-based models tend to focus on perceptual aspects rather than the fidelity of the reconstructed images, such as the essential structural information that is critical for clinical diagnosis.

To enhance fidelity, some works applied estimation information, such as depth maps and segmentation maps, to guide learning [14], [17], [18]. Ratul *et al.* [14] used additional organ segmentation maps to provide depth information for improved CT reconstruction. Ge *et al.* [17] designed a set of multi-task learning strategies to enhance CT reconstruction by coupling the reconstruction network with the segmentation network. These methods aim to learn the X-ray image to CT mapping in an end-to-end manner, guided by estimated information. However, the reliance on the accuracy of estimation limits their clinical values.

Mainstream GAN-based methods suffer from low fidelity, while CNN-based methods do not ensure optimal perceptual quality. In this paper, we introduce a new perspective to the challenging 2D-X-ray-to-3D-CT task by decomposing it into simpler sub-tasks, thereby significantly reducing learning difficulty and achieving a balance between fidelity and perceptual quality. Our novel task decomposition involves synthesizing new views using readily available view parameters in clinical diagnostics, translating intricate 2D-to-3D mapping into a more feasible 3D-to-3D latent space mapping, and then reconstructing and refining CT volumes. We anticipate that this strategy of task decomposition could provide a new learning paradigm for CT reconstruction field.

### B. Few-view 3D Reconstruction in Natural Images

Similar to X-ray-to-CT task, few-view 3D reconstruction task in natural images aims to recover the 3D structural from a limited number of 2D images. Due to the limited view information, traditional 3D reconstruction methods using polar constraints [21] cannot accurately determine spatial information. Recently, diffusion models [22] have achieved state-of-the-art results in several image generation tasks [23]–[28], including 3D reconstruction from few-view 2D images [29]–[35]. Some classical approaches typically use NeRF as the 3D representation and 2D diffusion model as a prior for reconstruction [31]–[33]. However, these approaches focus on reconstructing individual scenes and lack generalization to other images and scenes. Some works utilized additional learning networks to achieve generalized generation [36], [37].

Although diffusion models in natural images can be optimized for NeRF to achieve few-view 3D reconstruction, the NeRF-based approach is not directly applicable to CT reconstruction from X-rays. This is due to the penetration of X-rays through most objects, which results in the superimposition of different structures onto a 2D image. Consequently, the methods for extracting 3D models from X-ray images differ significantly from those employed in natural images. Additionally, NeRF-based implicit reconstruction methods can only capture the external shape and are unable to obtain the internal 3D details required for CT reconstruction. Corona *et al.* [16] proposed the MedNeRF model for synthesizing CT projections, but it can only generate new-view CT projections without reconstructing the internal details of the CT. Different from above methods, We build a 3D diffusion model for explicit CT reconstruction via denoising sampling, including both external contours and internal details.

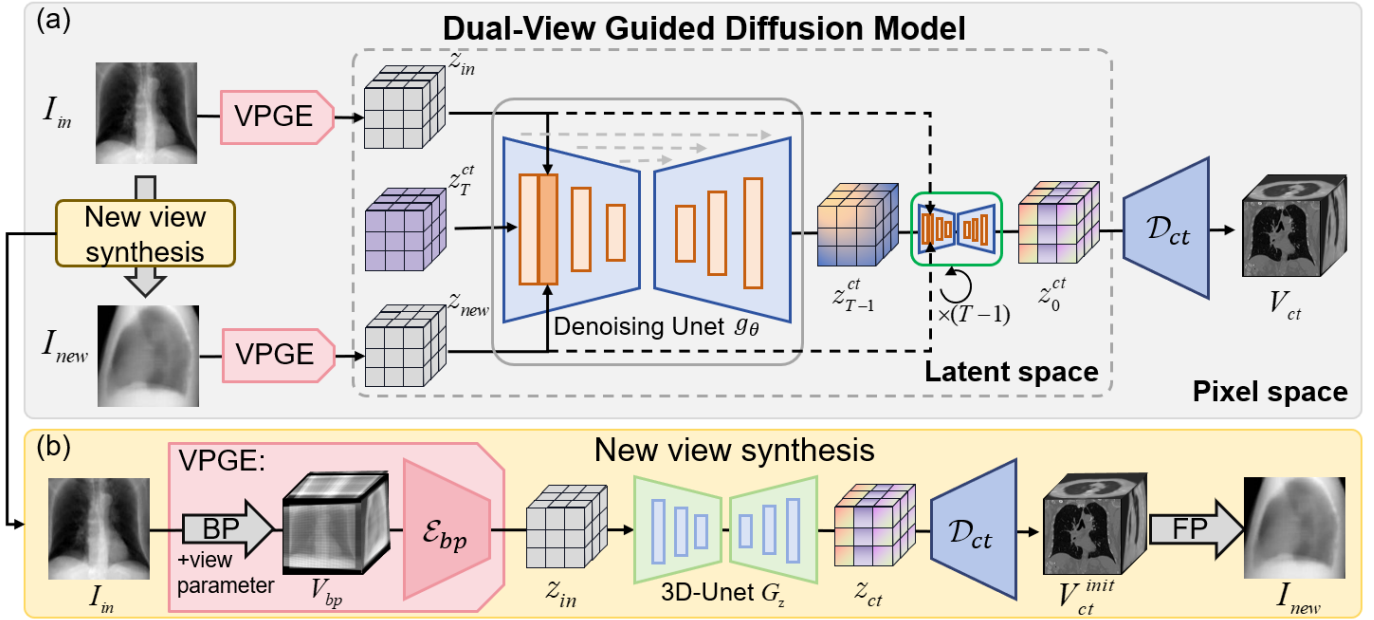


Fig. 1. Framework of the proposed DVG-Diffusion. (a) We utilize dual-view (i.e., the real input view  $I_{in}$  and the synthesized new view  $I_{new}$ ) to jointly guide the reconstruction of the finer CT volume ( $V_{ct}$ ).  $I_{in}$  and  $I_{new}$  are used as conditions to guide diffusion models to restore more detail. (b) We synthesize the new view ( $I_{new}$ ) by predicting the initial CT volume from the input view ( $I_{in} \rightarrow V_{ct}^{init}$ ) and then forward projecting the predicted CT to the new view X-ray ( $V_{ct}^{init} \rightarrow I_{new}$ ). A core design is our view parameter guided encoder (VPGE). To more easily align the feature space and learn the mapping from 2D images to 3D CT volume, in our VPGE, the input X-rays are first back projected into 3D space and then encoded into latent space ( $I_{in} \rightarrow V_{bp} \rightarrow z_{in}$ ).

### III. PROPOSED METHOD

Compared to a single X-ray image, biplanar X-rays can reconstruct higher quality CT volumes. This superiority stems from introducing additional views. These views provide complementary information and facilitate the transition from 2D X-rays to 3D CT volumes. Inspired by this, we propose a dual-view guided diffusion model (DVG-Diffusion) for CT reconstruction from X-rays (see Fig. 1). The “dual view guided” in our paper has two meanings. The first is reflected in view parameter guidance in feature encoder and view guided diffusion model in CT reconstruction. The second is manifested in using real-view and generated new-view to guide CT reconstruction. This dual view guided mechanism can achieve a good balance between high fidelity and high perceptual quality for CT reconstruction.

#### A. Overall Framework

Our DVG-Diffusion consists of three steps (see Fig. 1(a)). (1) Feature extraction: We propose a view parameter-guided encoder (VPGE) to extract latent features  $z_{in}$  and  $z_{new}$  from the input view  $I_{in}$  and new view  $I_{new}$ . (2) Feature transformation: We concatenate the features  $z_{in}$  and  $z_{new}$  as conditions for the diffusion model [22], using these dual view features to collaboratively guide the inverse generation of the latent representation of CT (denoted as  $z_0^{ct}$ ). (3) Feature decoding: We decode  $z_0^{ct}$  into pixel space to reconstruct the CT volume (denoted as  $V_{ct}$ ). For new view synthesis in Fig. 1(b), we synthesize the new view  $I_{new}$  by predicting the initial CT volume  $V_{ct}^{init}$  from the input real view  $I_{in}$  and then forward projecting  $V_{ct}^{init}$  to the new X-ray view  $I_{new}$  (the details in Section III-D).

#### B. Feature Extraction

Directly mapping 2D X-ray images to 3D CT volumes is imposed due to the lack of one-to-one correspondence between modalities. Unlike previous Diffusion-based methods [38]–[40] that directly encode input images end-to-end, we propose a novel **view parameter guided encoder** (VPGE) to better exploit the inherent structure and geometrical relationships between two modalities. In VPGE, the input X-rays are first back-projected into 3D space and then encoded into latent space to more easily align and learn the mapping from X-ray to CT. This process involves the following two steps:

1) We back-project a given 2D X-ray image  $I_{in} \in \mathbb{R}^{H \times W}$  into 3D space ( $\mathbb{R}^{H \times W \times D}$ ) to obtain  $V_{bp}$ .  $V_{bp} = BP(I_{in}, M)$ , where  $BP$  is the backprojector from [41]. It can properly place the X-ray image in 3D space while maintaining geometrical consistency:

$$BP(I_{in}, M) := \begin{cases} I_{in}/(|L|\Delta p), & My \in L, \\ 0, & otherwise, \end{cases} \quad (1)$$

where  $M$  represents the view parameter matrix controlling rotation and translation,  $L$  denotes line geometry constraints,  $\Delta p$  denotes sample step, and  $y$  denotes the coordinate point in 3D CT volume. To extend the backprojector to accept multi-view inputs, we back-project each input image separately and sum them together:

$$V_{bp} = \sum_{i=0}^n V_{bp}^i = \sum_{i=0}^i BP(I_{in}^i, M_i), \quad (2)$$

where  $n$  is the total number of input views, and  $I_{in}^i$  denotes the  $i$ -th input image. An example of a visual back-projection for

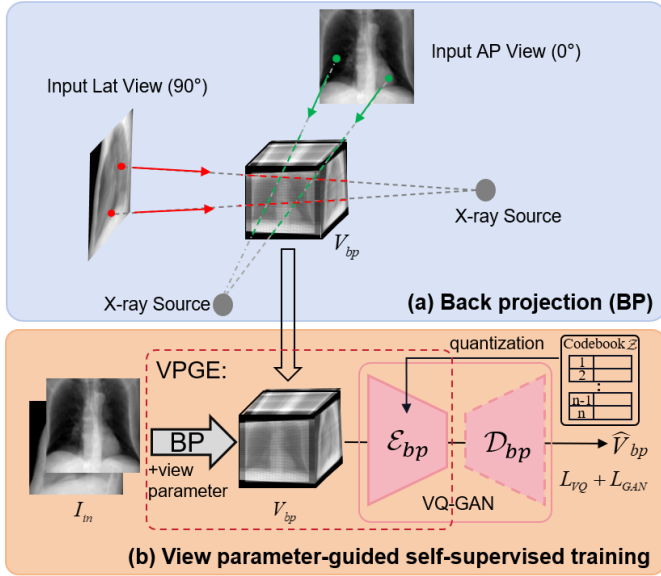


Fig. 2. The detailed process of back projection and VPGE using biplanar inputs as an example. The backprojector (BP) unfolds the points on each 2D projection into 3D space separately and superimposes them to obtain a geometrically consistent 3D image  $V_{bp}$ . The robust discrete feature encoder  $\mathcal{E}_{bp}$  is then obtained by self-supervised training of VQ-GAN.

biplanar inputs is presented in Fig. 2(a). This backprojection process incorporates the physical view information of the input X-ray images into the encoding process, which allows for better alignment of the representation space.

2) To fully exploit the inherent structure and geometrical relationships between X-ray and CT modalities, we employ a specialized encoder for the back-projected X-ray (denoted as  $V_{bp}$ ). This encoder, based on a self-supervised VQGAN [42], transforms  $V_{bp}$  into a latent space, represented as  $z_{in}$ , where  $z_{in} = \mathcal{E}_{bp}(V_{bp})$ . We uniformly use  $\mathcal{E}_{bp}(\cdot)$  to denote the CNN encoder  $E(\cdot)$  and quantization  $q(\cdot)$ .

The detailed flow of the encoder is shown in Fig. 2. Specifically, we encode the  $V_{bp}$  as a latent code  $\hat{z}_{in}$  using  $\hat{z}_{in} = E(V_{bp}) \in \mathbb{R}^{(H/f) \times (W/f) \times (D/f) \times n}$ , where  $n$  is the dimension of the codes, and  $f$  denotes a compression factor. Next, we perform element-wise quantization  $q(\hat{z}_{in})$  on each code in  $\hat{z}_{in}$ , mapping it to a pre-learned discrete codebook  $\mathcal{Z} = \{z_k\}_{k=1}^K$  as:

$$z_{in} = q(\hat{z}_{in}) = (\arg \min_{z_k \in \mathcal{Z}} \|\hat{z}_{in}^{ij} - z_k\|) \in \mathbb{R}^{h*w*d*n}, \quad (3)$$

where  $h = H/f$ ,  $w = W/f$ ,  $d = D/f$ .  $\hat{z}_{in}^{ij}$  denotes pixel value of row  $i$  and column  $j$  on  $\hat{z}_{in}$ . The reconstruction of  $\hat{V}_{bp} \approx V_{bp}$  is performed by a CNN decoder  $\mathcal{D}_{bp}$  based on the  $z_{in}$ , i.e.,  $\hat{V}_{bp} = \mathcal{D}_{bp}(z_{in}) = \mathcal{D}_{bp}(q(\hat{z}_{in}))$ .

In summary, our feature extraction stage employs the proposed VPGE to extract robust latent space features  $z_{in}$  and  $z_{new}$  from the input view  $I_{in}$  and new view  $I_{new}$ , respectively.

### C. Feature Transformation and Decoding

To efficiently process CT volume features and enhance their perceptual quality, we train a denoising UNet  $g_\theta$  to learn the target latent representation of CT (denoted as  $z_0^{ct}$ ). The

network  $g_\theta$  uses the features of input and new views ( $z_{in}$  and  $z_{new}$ ) as conditions to stepwise guide and transform  $z_T^{ct}$  (pure Gaussian noise) into  $z_0^{ct}$  (clear CT representation):

$$z_{t-1}^{ct} = \frac{1}{\sqrt{\alpha_t}} \left( z_t^{ct} - \frac{1 - \alpha_t}{1 - \bar{\alpha}_t} (z_t^{ct} - \sqrt{\bar{\alpha}_t} g_\theta(z_t^{ct}, z_{in}, z_{new}, t)) \right). \quad (4)$$

Where  $t$  is time step and uniformly sampled from  $\{1, 2, \dots, T\}$ ,  $z_t^{ct}$  can be obtained by adding Gaussian noise to  $z_0^{ct}$  in the forward process with a fixed cosine schedule [22]:

$$q(z_t^{ct} | z_{t-1}^{ct}) \sim \mathcal{N}(z_t^{ct}; \sqrt{\alpha_t} z_{t-1}^{ct}, (1 - \alpha_t) \mathbf{I}). \quad (5)$$

The denoising network  $g_\theta$  is trained for estimating  $z_0^{ct}$ , and supervised by Mean Square Error (MSE) loss:

$$L_{diff} := \|g_\theta(z_t^{ct}, z_{in}, z_{new}, t) - z_0^{ct}\|_2^2. \quad (6)$$

With iterative sampling in Eq. 4, we obtain the CT latent representation  $z_0^{ct}$ . Subsequently, the CT volume  $V_{ct}$  is reconstructed by decoding  $z_0^{ct}$  into pixel space by a decoder  $\mathcal{D}_{ct}$  specialized for 3D CT volumes via VQGAN [43].

Using diffusion models for CT reconstruction can substantially enhance perceptual performance. However, the stochastic nature of the denoising process may result in the generated samples lacking fidelity. In our method, the feature  $z_{new}$  is extracted from the new view  $I_{new}$ , which is mined completely from the input X-ray image to improve data utilization efficiency. This provides stronger spatial constraints for the denoising process, facilitating the reconstruction of finer CT volumes with 3D consistency. In the following section, we describe the process of synthesizing new view  $I_{new}$  from input view  $I_{in}$ .

### D. New X-ray View Synthesis

To obtain X-ray images with more 3D consistency, our new view synthesis is not achieved through a simple 2D-to-2D mapping. Instead, it relies on the VPGE module to leverage the 3D information from CT volume, enabling a more reliable 2D-to-3D-to-2D mapping.

Given an input X-ray  $I_{in}$ , our VPGE-based new view synthesis utilizes the following image processing pipeline:

$$I_{in} \xrightarrow{BP} V_{bp} \xrightarrow{\mathcal{E}_{bp}(V_{bp})} z_{in} \xrightarrow{G_z(z_{in})} z_{ct} \xrightarrow{\mathcal{D}_{ct}(z_{ct})} V_{ct} \xrightarrow{FP} I_{new}. \quad (7)$$

$G_z$  is realized as a 3DUNet [43] to map the feature of input real views  $z_{in}$  to the latent representation of initial CT volume (denoted as  $z_{ct}$ ), and is supervised by following loss:

$$L_{rec} := \|G_z(z_{in}) - z_{ct}^{gt}\|_2^2. \quad (8)$$

$\mathcal{D}_{ct}$  is a decoder specialized for 3D CT volumes via VQGAN [43] without BP projection. We employed the same VQGAN architecture for both CT encoding/decoding and  $V_{bp}$  encoding/decoding, ensuring spatially coherent representation between two modalities.

We obtain the new view by  $I_{new} = FP(V_{ct}, M_{new})$ , where  $M_{new}$  represents the parameter matrix of the new view  $I_{new}$ , and  $FP$  is a differentiable forward projector [41] for CT-to-X-ray:

$$FP(V_{ct}, M_{new}) := \int V_{ct}(M_{new}^{-1}p) dL \approx \sum_{p \in L} V_{ct}(M_{new}^{-1}p) \Delta p. \quad (9)$$

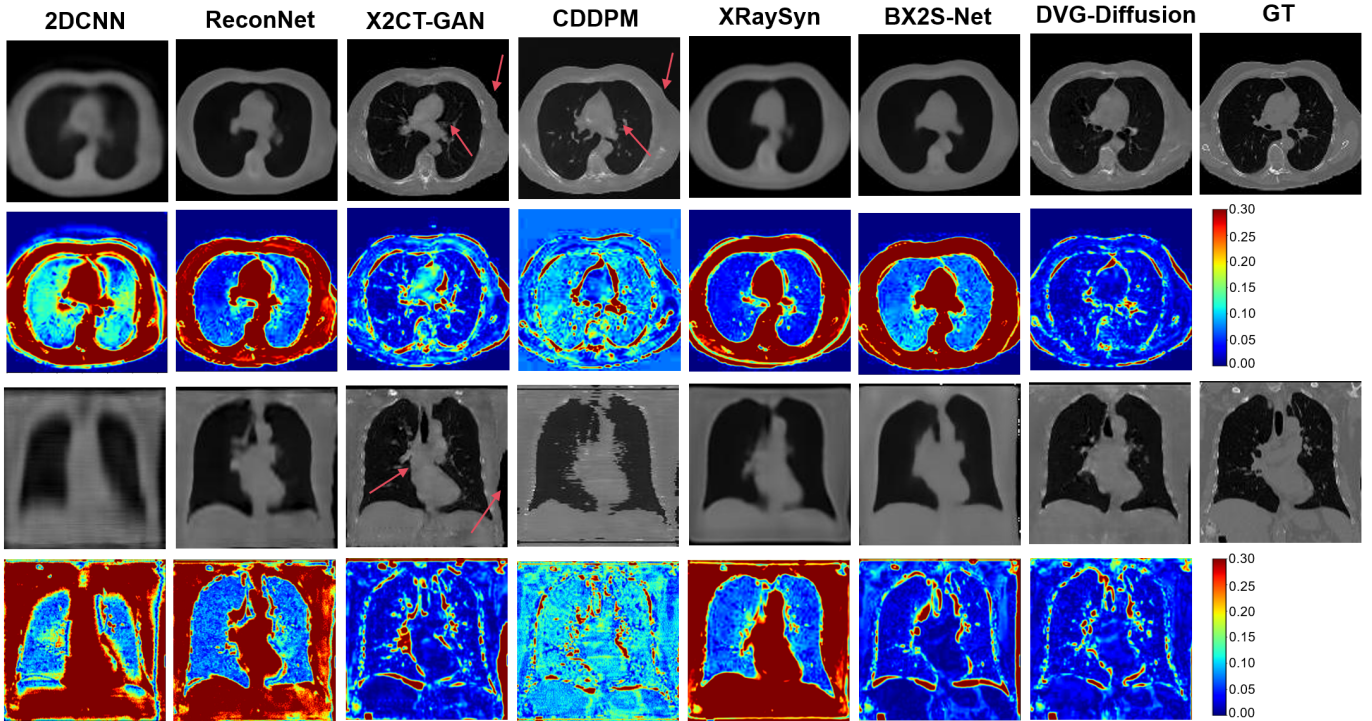


Fig. 3. Example of reconstructed CT slices from biplanar X-rays using the proposed DVG-Diffusion and competing methods, along with the prediction error maps. Two sets of samples are slices along the axial plane (AXI) and coronal plane (COR). Red arrows in the figure indicate instances of contour distortion.

Our view synthesis network captures features from X-rays aligned as closely as possible with CT via VPGE, facilitating the reconstruction of initial CT volumes with better 3D consistency. It synthesizes a reliable new view  $I_{new}$  that is then fed into dual view guided diffusion model for finer CT reconstruction.

#### IV. EXPERIMENTS AND RESULTS

In this section, we first introduce the experimental implementation details. Then, we compare our DVG-Diffusion with several state-of-the-art methods and conduct ablation studies to validate our model.

##### A. Experimental Setup

**Dataset:** We evaluated our method on the LIDC-IDRI dataset [44], containing 1018 chest CT volumes. Following [41], we synthesized corresponding X-ray images of different views from real CT volumes using the differentiable forward projector (FP) [41]. We randomly selected 916 CT volumes for training, and used the remaining 102 volumes for testing. We followed the pipeline introduced in [13] for CT volume pre-processing.

**Implementation Details:** Two sets of experiments were conducted: (1) CT reconstruction from single-view X-ray, where we used Anterior-Posterior (AP) view, and (2) CT reconstruction from biplanar X-rays, where we used both Anterior-Posterior (AP) and Lateral (Lat) views. We implemented our models using PyTorch on a single NVIDIA 4090 24GB GPU, with a batch size of 2 and the Adam optimizer [45].

The implementation of different stages in our model is as follows: **(1) For VQGAN:** For CT encoding/decoding, the learning rate was set to  $3 \times 10^{-4}$ , and training was conducted over 100 epochs. In contrast, for  $V_{bp}$  encoding/decoding, the learning rate was the same, but the training epoch was set to 50. **(2) For diffusion model:** We adopted the 3D UNet from [43] as our denoising model. We set the total diffusion timesteps to 100 and used a learning rate of  $2 \times 10^{-4}$ . **(3) For new view synthesis:** For CT reconstruction from single view X-ray, we used the input AP view (set to  $0^\circ$ ) to synthesize Lat View ( $90^\circ$ ). For biplanar X-rays, we used the input AP view and Lat view to synthesize the middle ( $45^\circ$ ) view.

**Comparison Methods and Evaluation Metrics:** We compared our DVG-Diffusion with four CNN-based approaches (2DCNN [20], ReconNet [15], XRaySyn [41] and BX2S-Net [3]), one GAN-based approach (X2CT-GAN [13]), and one conditional diffusion model (CDDPM [46]). In particular, for the XRaySyn [41] model, we evaluated the CT reconstruction network (3DPriorNet). CDDPM [46] is a conditional diffusion model with our own implementation, conditioned on the back-projection of the X-ray image.

We evaluated the performance of these methods with two distortion metrics (Peak Signal-to-Noise Ratio (PSNR), Structured Similarity Index (SSIM)), and one perceptual metric (Learned Perceptual Image Patch Similarity (LPIPS) [47]). PSNR and SSIM primarily assess overall image quality, whereas LPIPS evaluates perceptual details at the feature level.

##### B. Comparison Results

We present the comparison results in Fig. 3 and Table I. It is widely recognized that CNN-based methods typically

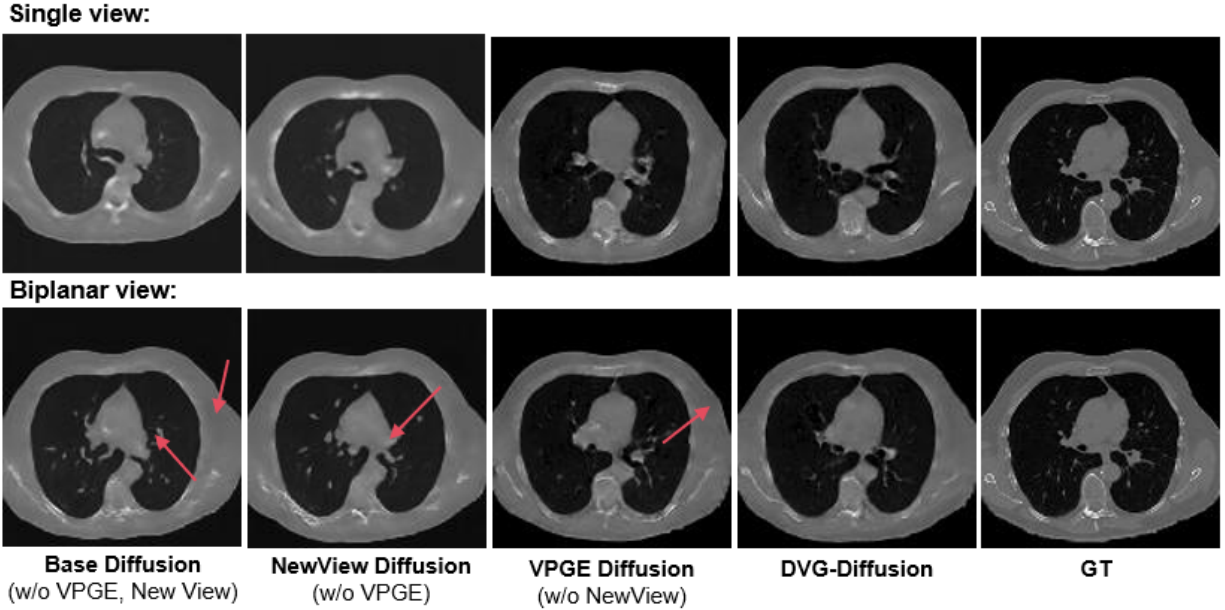


Fig. 4. Visual results of baseline and the proposed DVG-Diffusion in ablation studies, using single-view and biplanar X-rays as inputs.

TABLE I  
QUANTITATIVE COMPARISON OF FIVE CT RECONSTRUCTION METHODS USING SINGLE-VIEW X-RAY AND BIPLANAR X-RAYS AS INPUTS, RESPECTIVELY. **BOLDING** AND UNDERLINE DENOTE THE BEST AND THE SECOND BEST RESULT, RESPECTIVELY.

Method	Single-view X-ray			Biplanar X-rays		
	PSNR $\uparrow$	SSIM $\uparrow$	LPIPS $\downarrow$	PSNR $\uparrow$	SSIM $\uparrow$	LPIPS $\downarrow$
2DCNN [20]	19.01	0.480	49.71	22.85	0.595	46.05
ReconNet [15]	21.35	0.521	46.53	24.01	0.625	40.70
X2CT-GAN [13]	21.40	0.505	39.62	24.82	0.613	31.73
XRaysyn [41]	21.07	<b>0.558</b>	46.20	24.45	<b>0.684</b>	39.43
CDDPM [46]	20.05	0.508	46.95	22.04	0.610	41.16
BX2S-Net [3]	21.19	<b>0.558</b>	44.65	24.69	0.658	38.88
DVG-Diffusion (Ours)	<b>22.54</b>	<u>0.541</u>	<b>36.79</b>	<b>26.84</b>	<u>0.679</u>	<b>27.35</b>

excel in generating images with good distortion metrics, while GAN-based methods are adept at capturing perceptual details [13]. Achieving a balance between perceptual and distortion metrics in X-rays-to-CT generation remains a challenging task. As shown in Table I and Fig. 3, among all the compared baselines, the CNN methods XRaysyn and BX2S-Net deliver the top results on the distortion metric SSIM, despite their perceptual quality being subpar. The GAN-based X2CT-GAN performs well in the perceptual metric LPIPS but struggles with maintaining distortion accuracy. This trade-off is also evident in Fig. 3 (marked with red arrows), where the contour structure of the CT image generated by X2CT-GAN exhibits significant distortion. Furthermore, samples produced by the CNN method appear too smooth and lack detail, resulting in a substantial gap in overall quality compared to the ground truth, as shown by the error maps. In contrast, our proposed DVG-Diffusion method successfully achieves a good balance between high fidelity and perceptual quality in CT reconstruction, resulting in the best performance among all competing methods in both perceptual and distortion metrics.

### C. Results of Ablation Experiments

This section investigates the effects of VPGE and the new view synthesis guidance in DVG-Diffusion. We remove each

of these modules from the DVG-Diffusion model individually and evaluate the resulting variants: Base-Diffusion (both VPGE and new view synthesis guidance removed), NewView-Diffusion (VPGE removed), and VPGE-Diffusion (new view synthesis guidance removed). All derived models were trained using a strategy similar to our DVG-Diffusion. Results are presented in Table II and Fig. 4.

**Effectiveness of VPGE:** Directly mapping 2D X-ray images to 3D CT volumes is inherently ill-posed due to the lack of one-to-one correspondence between the two modalities. This challenge is evident in the lowest performance of the Base-Diffusion variant (see Table II). By incorporating the VPGE module into the Base-Diffusion model, we simplify the decomposition of the original complex end-to-end 2D to 3D mapping. VPGE pre-codes the X-ray images and constructs a more feasible 3D to 3D latent spatial mapping, which leads to a significant improvement in performance (comparing Base-Diffusion and VPGE-Diffusion).

**Effectiveness of new view synthesis guidance:** Removing the new view synthesis guidance from our DVG-Diffusion method results in a noticeable decrease in image fidelity, as evidenced by the SSIM distortion metric, which drops from 0.679 in our DVG-Diffusion with biplanar inputs to 0.667 in the VPGE-Diffusion variant. This reduction is also evident in

TABLE II

ABLATION STUDY TO EVALUATE THE IMPACT OF VPGE AND NEW VIEW SYNTHESIS GUIDANCE MODULES IN DVG-DIFFUSION, USING SINGLE VIEW AND BIPLANAR X-RAYS AS INPUTS.

	VPGE	New View	Single	Biplanar	PSNR $\uparrow$	SSIM $\uparrow$	LPIPS $\downarrow$
Base-Diffusion	-	-	✓		20.05	0.508	46.95
NewView-Diffusion	-	✓	✓		20.62	0.519	44.67
VPGE-Diffusion	✓	-	✓		22.29	0.532	37.59
DVG-Diffusion (Ours)	✓	✓	✓		<b>22.54</b>	<b>0.541</b>	<b>36.79</b>
Base-Diffusion	-	-		✓	22.04	0.610	41.16
NewView-Diffusion	-	✓		✓	22.53	0.625	39.85
VPGE-Diffusion	✓	-		✓	26.47	0.667	28.11
DVG-Diffusion (Ours)	✓	✓		✓	<b>26.84</b>	<b>0.679</b>	<b>27.35</b>

Fig. 4 (marked by red arrows), where the image generated by the VPGE-Diffusion variant exhibits noticeable distortion in the contour structure. In contrast, the use of our proposed new view synthesis guidance greatly improves image fidelity by providing supplementary new view X-ray images as guidance.

## V. DISCUSSION

### A. Impact of X-ray Quantity and Angular Distribution on CT Reconstruction

In our experiments, we tested the performance of our DVG-Diffusion method in two experimental settings: CT reconstruction from single-view X-ray and biplanar X-rays. Intuitively, using more input views can lead to better 3D CT reconstruction. However, increasing the number of input X-ray views also introduces additional costs, such as increased acquisition time and computational complexity. Selecting the optimal parameters that balance reconstruction quality and cost is a crucial challenge. Moreover, for a given number of input views, the performance of CT reconstruction may vary depending on the angular distribution of the views.

In this section, we conduct extensive experiments to explore the impact of the number of input views and angular distribution on CT reconstruction quality. Specifically, we conducted a series of experiments with different numbers of input views, ranging from 1 to 20. We uniformly sampled the expected number of input X-ray views from two view ranges:  $0^\circ$ - $90^\circ$  and  $0^\circ$ - $360^\circ$ , with the first input view set as the Anterior-Posterior (AP). These ranges,  $0^\circ$ - $90^\circ$  and  $0^\circ$ - $360^\circ$ , are two common sampling ranges for CT reconstruction from X-ray, referred to as limited angle CT and sparse-view CT [48]. To accurately evaluate the performance of view quantity and view selection on CT reconstruction, we removed the new-view synthesis module in DVG-Diffusion to eliminate the influence of synthesized new views on the final performance. Moreover, we compared our method with one of the SOTA CT reconstruction methods, ReconNet [15], to validate the superiority of DVG-Diffusion. Other comparison methods listed in Table I were specifically designed for single-plane or biplanar X-rays and therefore are not involved in this comparison.

**Observation I: Superior CT reconstruction performance with  $90^\circ$  sampling than  $360^\circ$  for few-view inputs.** Fig. 5 compares the performance of DVG-Diffusion for reconstructions using around  $360^\circ$  and around  $90^\circ$  views, showing that with fewer than 10 views, sampling around the  $90^\circ$  range yields better reconstruction results than sampling around the

$360^\circ$  range. The improved performance can be attributed to the way in which the input X-ray image is generated, a process known as forward projection (FP). This process involves integrating samples along the projection line, resulting in similar information for symmetrical regions. Consequently, it is easier to sample duplicate information in  $360^\circ$  when the number of sampled input views is limited. X-ray images sampled within the orthogonal view range ( $90^\circ$ ) contain more comprehensive information, leading to enhanced performance compared to those sampled around  $360^\circ$ . This observation is further supported by Figure 6, where images sampled from the  $90^\circ$  range reveal the basic shape contours of CT in back projection (BP) more rapidly than those sampled from the  $360^\circ$  range (see the 4-view examples). Our new-view synthesis experiment is also based on these findings, suggesting that the angle for synthesizing new X-ray views should ideally be selected within the  $90^\circ$  range. However, as the number of views increases, the  $360^\circ$  sampling gradually outperforms the  $90^\circ$  sampling. This occurs because the information within the  $90^\circ$  range becomes fully exploited, necessitating a broader range of spatial information for achieving a more detailed reconstruction.

**Observation II: Inflection points in reconstruction performance occur at 3 and 8 inputs.** In this experimental section, we further explore the impact of different numbers of input views on the CT reconstruction performance, focusing on a  $90^\circ$  sampling range. Fig. 5 indicates that the reconstruction performance of DVG-Diffusion displays a noticeable inflection point when the number of input views changes. In particular, inflection points in the reconstruction performance are observed at 3 and 8 inputs. When the number of input views is less than 3, we observe a rapid improvement in the reconstruction performance as each additional view is included. The information from these initial views is crucial, as they provide the fundamental structure and orientation details necessary for the reconstruction. However, as the number of input views increases from 3 to 8, the rate of improvement in reconstruction performance begins to slow down. This is because the additional views provide increasingly overlapping or redundant information, which contributes less to the overall quality of the reconstruction. This experiment offers insights into the number of synthesized views required, which will be further discussed in Section V-B.

**Observation III: Our method demonstrates robustness as the number of X-ray image inputs increases.** We compare the performance of DVG-Diffusion with ReconNet, focusing

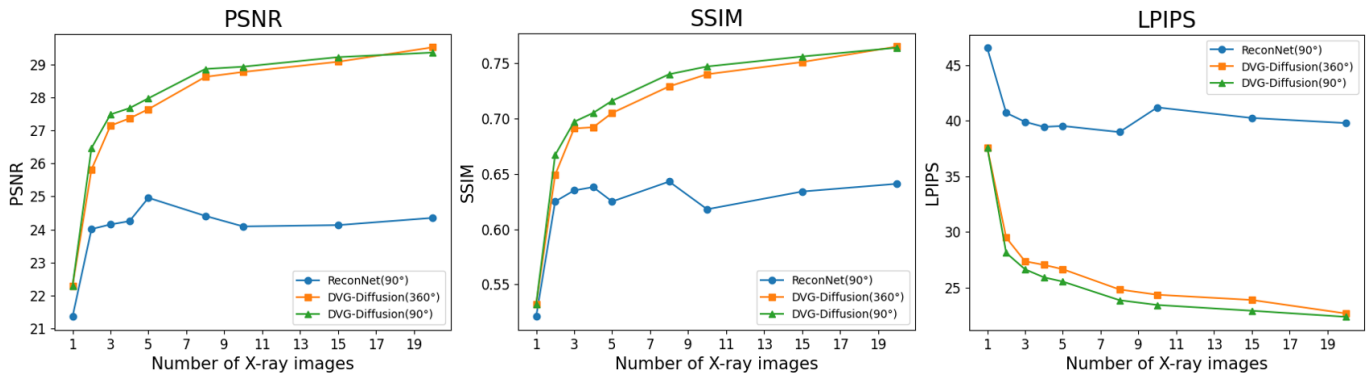


Fig. 5. Performance curves of CT reconstruction using DVG-Diffusion (without new view synthesis) for different numbers of input views and different angle sampling ranges, and a comparison with ReconNet.

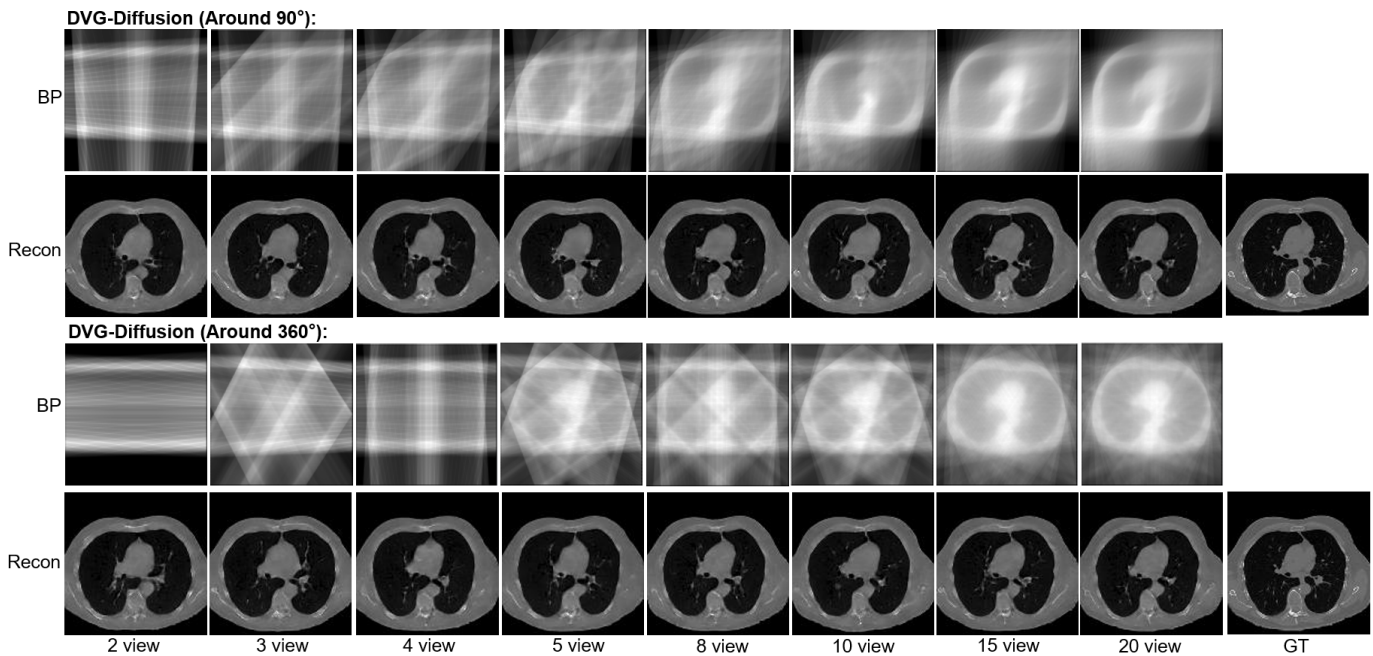


Fig. 6. Visual results of CT reconstruction using DVG-Diffusion (without new view synthesis) for different numbers of input views and different angle sampling ranges.

on a  $90^\circ$  sampling range. As shown in Fig. 5, our method leads across the board in fidelity (PSNR, SSIM) and perceptual (LPIPS) metrics as the number of inputs increases. We find that the CT reconstruction performance of ReconNet plateaus and does not improve further when the number of input views exceeds five. In contrast, our DVG-Diffusion model exhibits a steady enhancement in performance with an increasing number of input views. This observation demonstrates the effectiveness of the VPGE module and the efficient diffusion model learning strategy in our DVG-diffusion model. These designs enable our model to effectively handle different numbers of input views and obtain robust reconstruction quality.

### B. An In-Depth Analysis of the New View Synthesis

The superiority of our DVG-Diffusion model can be attributed to three key components: the efficient VPGE module, the innovative new view synthesis, and the robust dual-view

TABLE III  
QUANTITATIVE RESULTS OF CT RECONSTRUCTION GUIDED BY SYNTHESIZING A NEW VIEW WITH DIFFERENT ANGLES WHEN SINGLE-VIEW X-RAY INPUT. (THE INPUT VIEW IS AN AP ( $0^\circ$ ) VIEW.) W/O DENOTES NO NEW VIEW INPUT.

	w/o	$10^\circ$	$30^\circ$	$45^\circ$	$60^\circ$	$90^\circ$	$120^\circ$
PSNR $\uparrow$	22.29	22.46	22.47	22.43	22.48	<b>22.54</b>	22.47
SSIM $\uparrow$	0.532	0.537	0.539	0.540	0.539	<b>0.541</b>	0.537
LPIPS $\downarrow$	37.59	37.11	36.84	37.08	37.15	<b>36.79</b>	37.23

guided diffusion model. We established the effectiveness of these individual components in Section IV-C. In this section, we conduct extensive experiments to unravel the impact of the new view synthesis on CT reconstruction performance. Specifically, we verified three key aspects: (1) the optimal angle for new view synthesis that yields the most favorable results for final CT reconstruction; (2) the ideal number of synthesized new views required to achieve the best CT

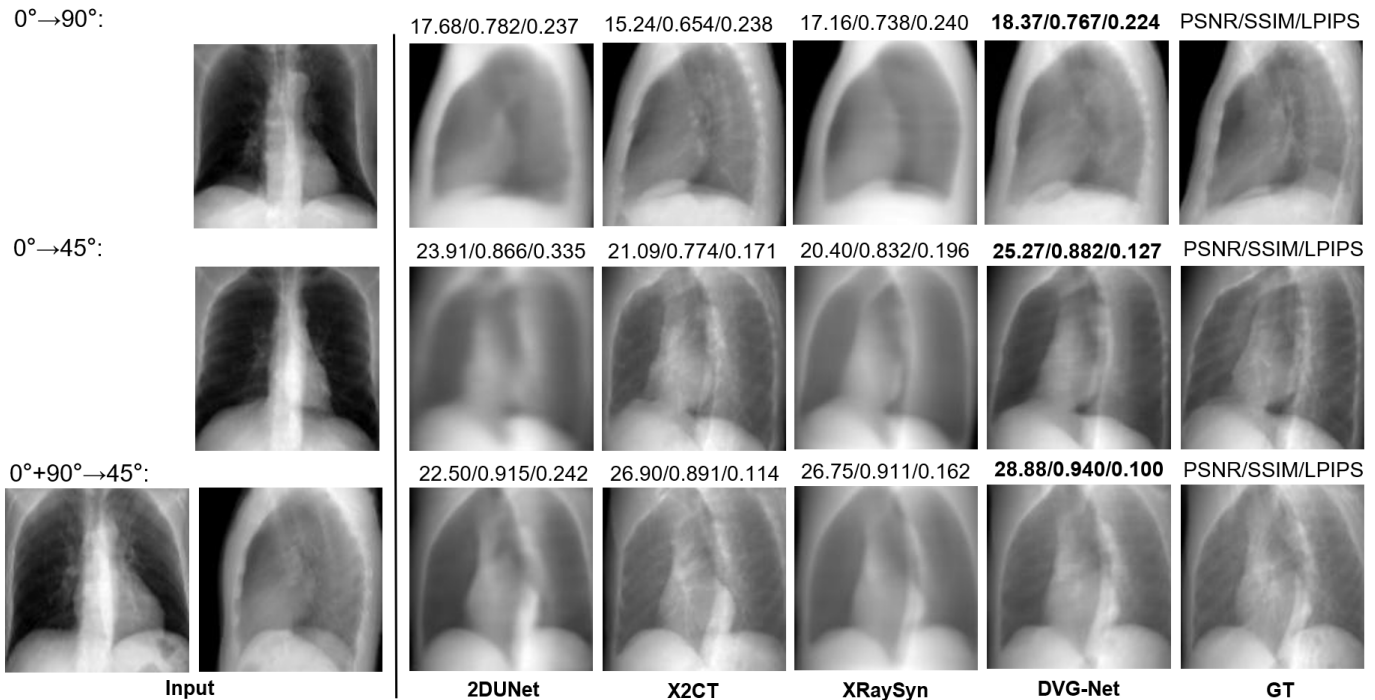


Fig. 7. Visual results of new view synthesis using the proposed DVG-Diffusion (New View Synthesis Stage) and other comparison methods.

TABLE IV  
EXPERIMENTAL SETTINGS FOR NEW VIEW SYNTHESIS BASED ON DIFFERENT INPUT VIEWS.

input view	single-view	two-view	three-view
input angle	0°	0°, 90°	0°, 45°, 90°
1 new view	90°	45°	22.5°
2 new view	45°, 90°	22.5°, 67.5°	22.5°, 67.5°

reconstruction; and (3) the superior performance of new view synthesis in comparison to other methods.

**Observation IV: Synthesizing orthogonal view brings the best performance gains for a single view input.** In our previous observation, we demonstrated superior CT reconstruction performance with 90° sampling than 360° for few-view inputs. This suggests that the angle for synthesizing new X-ray views should ideally be selected within the 90° range. Here, we further investigate the new view synthesis for a single view input. As shown in Table III, the best CT reconstruction performance is achieved when generating the 90° views. Constructing orthogonal views (0° and 90°) leads to the greatest performance improvement, consistent with the study in Section V-A. Despite the best performance achieved when generating orthogonal view, our experiments also confirm that, for a given single view as input, generating new views at any angle still provides some improvement.

**Observation V: Enhanced performance of the new view synthesis with limited input views.** We investigate the performance of our DVG-Diffusion model when given a limited number of X-ray views as inputs, such as a single view, biplanar views, and three views. For each scenario, we synthesize 1, 2, and 3 new views and assess their impact on CT reconstruction. As per Observation I, the angles of these

new views are uniformly sampled within a 0-90° range, as detailed in Table IV. The results, presented in Table V, reveal that when only one or two real views are available as input, our new view synthesis improves CT reconstruction performance. However, when the number of real views increases to three or more, the addition of synthesized views does not further enhance the performance. This observation aligns with our previous experimental findings in Fig. 5, where the reconstruction performance improves substantially when three or fewer input views are provided and then adding real views, but the improvements taper off after three views. This suggests that when three or more input views are given, the model already obtains sufficient information from the existing real views, and the synthesized views do not contribute additional significant information. Based on these findings, we optimize our final model to synthesize one new view when given single-plane or biplanar inputs. No new views are synthesized when more planes are available as input. Despite the diminishing returns of our new view synthesis in CT reconstruction, our new view strategy is still quite useful in clinical scenarios, where typically only one or two X-ray views (Anterior-Posterior view (AP) and Lateral view (Lat)) are available. In cases where more views are available, our method still delivers excellent multi-view reconstruction performance through the effective coding capabilities of VPGE, as highlighted in Fig. 5.

**Observation VI: Superior new view synthesis performance compared with other methods.** Finally, we compare the performance of the X-ray images ( $I_{new}$ ) generated by the new view synthesis stage in our DVG-Diffusion model (referred to as DVG-Net) with other state-of-the-art methods. In this comparison, we include one 2D method (UNet with residual blocks [49]), two 3D methods (X2CT [13]

TABLE V  
PERFORMANCE OF CT RECONSTRUCTION USING DIFFERENT NUMBERS OF NEW VIEWS TO GUIDE CT RECONSTRUCTION WHEN DIFFERENT NUMBERS OF INPUT VIEWS ARE USED.

New views	single-view			two-view			three-view		
	PSNR $\uparrow$	SSIM $\uparrow$	LPIPS $\downarrow$	PSNR $\uparrow$	SSIM $\uparrow$	LPIPS $\downarrow$	PSNR $\uparrow$	SSIM $\uparrow$	LPIPS $\downarrow$
0	22.29	0.532	37.59	26.47	0.667	28.11	<b>27.49</b>	<b>0.697</b>	26.63
1	22.54	0.541	36.79	<b>26.84</b>	<b>0.679</b>	<b>27.35</b>	27.48	0.696	<b>26.58</b>
2	<b>22.59</b>	<b>0.543</b>	<b>36.57</b>	26.80	0.676	27.51	27.39	0.696	26.75

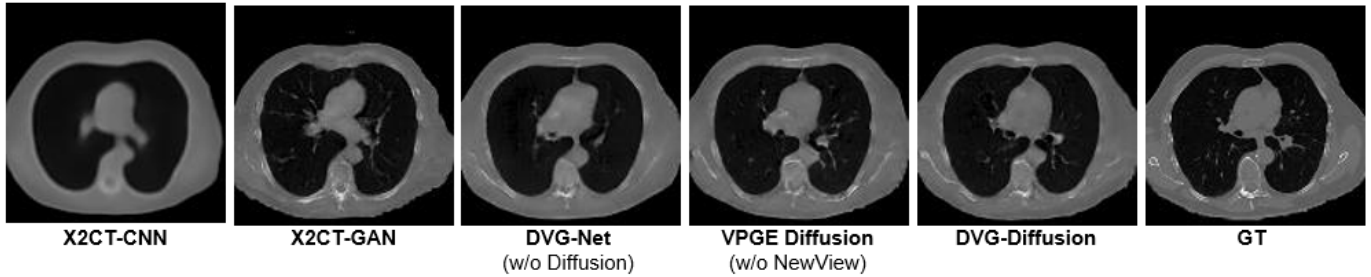


Fig. 8. Visual results of CT reconstruction using CNN methods and generative methods (GAN, Diffusion).

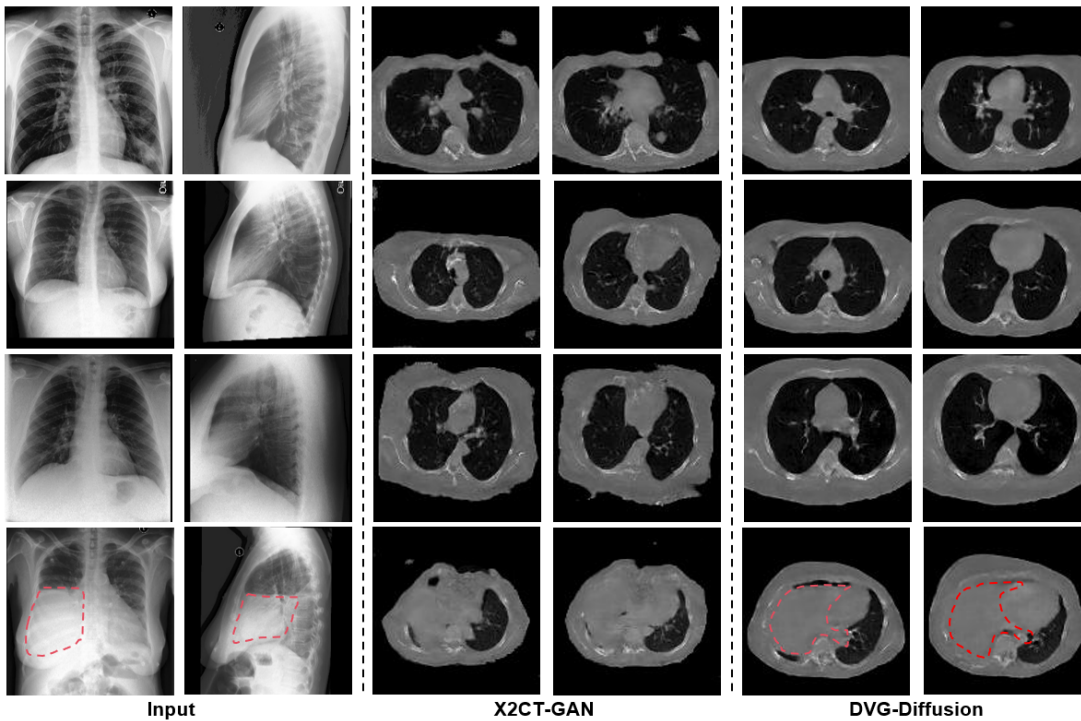


Fig. 9. Visual results of CT reconstruction using real-world biplanar X-ray images.

TABLE VI  
QUANTITATIVE RESULTS OF NEW VIEW SYNTHESIS USING THE PROPOSED DVG-DIFFUSION (NEW VIEW SYNTHESIS STAGE) AND OTHER COMPARISON METHODS.

		UNet	X2CT	XRaysyn	DVG-Net
$0^\circ \rightarrow 90^\circ$	PSNR $\uparrow$	18.57	17.77	17.15	<b>19.08</b>
	SSIM $\uparrow$	0.766	0.739	0.753	<b>0.778</b>
	LPIPS $\downarrow$	0.234	0.188	0.238	<b>0.186</b>
$0^\circ \rightarrow 45^\circ$	PSNR $\uparrow$	22.18	21.63	21.45	<b>22.58</b>
	SSIM $\uparrow$	<b>0.843</b>	0.799	0.824	0.842
	LPIPS $\downarrow$	0.294	0.154	0.196	<b>0.148</b>
$0^\circ + 90^\circ \rightarrow 45^\circ$	PSNR $\uparrow$	25.78	26.03	25.67	<b>27.43</b>
	SSIM $\uparrow$	0.911	0.883	0.910	<b>0.922</b>
	LPIPS $\downarrow$	0.240	0.118	0.161	<b>0.099</b>

and XRaysyn [41]). We present the results in Table VI and Fig. 7. The UNet method [49] is a 2D approach and learns the mapping between views directly, which limits its ability to capture and reconstruct reliable 3D information. As a result, the generated projections from UNet may lack essential depth and structural details. The X2CT method [13] aims to generate realistic samples using a GAN-based approach. While the overall appearance of the generated projections might be visually plausible, the method often struggles to maintain the fidelity of contours and intricate features, which are crucial for accurate CT reconstruction. The XRaysyn method [41] tends to produce synthesized samples that appear

overly smooth, causing them to miss essential details necessary for accurate reconstruction. This smoothing effect may lead to suboptimal CT reconstructions, as the algorithm struggles to model fine structures and subtle variations in the data. In contrast, our method consistently outperforms the other methods, as evidenced by the more accurate contours and detailed features in the synthesized projections. This superior performance highlights the effectiveness of our new view synthesis and its potential for improving CT reconstruction, especially in challenging scenarios with limited input views.

### C. Fidelity vs. Perceptual

In the task of CT reconstruction from few-view X-ray images, achieving a balance between fidelity and perceptual quality of the reconstructed CT volume remains a significant challenge. This issue is highlighted in [13], where two reconstruction approaches were proposed: (1) X2CT-CNN model, which employs a CNN-based method for reconstruction, and (2) X2CT-GAN model, which utilizes a generative GAN-based approach. As shown in Table VII, the X2CT-GAN model achieves better perceptual performance compared to X2CT-CNN (LPIPS decreased from 37.29 to 31.73), but at the cost of a significant reduction in fidelity (SSIM decreased from 0.682 to 0.613). This trade-off is also evident in Fig. 8, where the structures reconstructed by X2CT-GAN exhibit distortions, while those from X2CT-CNN appear overly smooth.

A similar challenge persists when applying diffusion models. Based on our proposed framework, we constructed three models for comparison: (1) DVG-Net model, which uses a CNN-based method (novel view generation stage) for reconstruction; (2) VPGE-Diffusion model, which employs a diffusion-based approach without additional synthesized views for guidance during our diffusion generation stage; and (3) our complete DVG-Diffusion model. As shown in Table VII, all three models outperform the X2CT series, benefiting from our proposed VPGE, which constructs an aligned latent space that reduces the difficulty of 2D-3D learning. However, purely diffusion-based VPGE-Diffusion model shows better perceptual metrics (LPIPS decreased from 29.50 to 28.11) but worse fidelity (SSIM decreased from 0.702 to 0.667) compared to the CNN-based DVG-Net. In contrast, our DVG-Diffusion model achieves a superior balance between these two aspects, maintaining high fidelity while significantly improving perceptual performance. This observation is further supported by Fig. 8, where the VPGE-Diffusion model produces CT volumes with higher visual quality but noticeable structural distortions, while the DVG-Net model reconstructs structures more accurately but suffers from over-smoothed details. Our proposed DVG-Diffusion model effectively combines the strengths of both approaches, delivering superior performance in both image detail and structural integrity. This is attributed to the use of additional new views for guidance in DVG-Diffusion, which are derived from the DVG-Net model’s superior structural information. By leveraging these high-quality structural features as guidance, DVG-Diffusion ensures precise CT volume reconstruction without compromising the inherent generative capabilities of the diffusion process.

TABLE VII  
PERFORMANCE COMPARISON OF CT RECONSTRUCTION BETWEEN CNN METHODS AND GENERATIVE METHODS (GAN, DIFFUSION).

View	Model	PSNR $\uparrow$	SSIM $\uparrow$	LPIPS $\downarrow$
Single	X2CT-CNN [13]	22.18	0.553	44.27
	X2CT-GAN [13]	21.40	0.505	39.62
	DVG-Net (Ours)	<b>23.08</b>	<b>0.568</b>	38.59
	VPGE-Diffusion (Ours)	22.29	0.532	37.59
	<b>DVG-Diffusion (Ours)</b>	22.54	0.541	<b>36.79</b>
Biplanar	X2CT-CNN [13]	26.34	0.682	37.29
	X2CT-GAN [13]	24.82	0.613	31.73
	DVG-Net (Ours)	<b>27.25</b>	<b>0.702</b>	29.50
	VPGE-Diffusion (Ours)	26.47	0.667	28.11
	<b>DVG-Diffusion (Ours)</b>	26.84	0.679	<b>27.35</b>

### D. Clinical Application

To validate the robustness of our model on real clinical data, we utilized authentic X-ray images obtained from clinical diagnoses in the MIMIC-CXR [50] dataset for CT reconstruction. In Figure 9, we present a visual comparison with X2CT-GAN [13]. Our method demonstrates superior reconstruction quality, generating CT images with more consistent volumetric structures and more well-defined boundary contours, even in real-world scenarios. Furthermore, when reconstructing images with pathological features (e.g., pleural effusion, as shown in the last row), our approach successfully reconstructs clearer 3D pathological features, providing more reliable guidance for surgical planning and prognosis. We attribute these improvements to the aligned latent space constructed by our method, which effectively bridges the gap between the two modalities. Additionally, the incorporation of supplementary views provides complementary information, mitigating potential spatial inconsistencies in real X-ray images and thereby stabilizing the CT reconstruction process.

### E. Limitations and Future Work

Our DVG-Diffusion model, while effective, has certain limitations. First, the model reconstructs by learning new views to guide the dual-view diffusion model. However, new view extraction takes place in pixel space, while the diffusion process occurs in latent space, necessitating a  $z_{ct} - V_{ct}^{init} - I_{new} - z_{new}$  (latent-pixel-latent) process that increases computational burden. Future work aims to streamline this pipeline by operating directly in the latent space, significantly reducing its complexity. Furthermore, although our current method achieves state-of-the-art performance, the new view remains subpar compared to the ground truth. As part of our ongoing efforts, we plan to explore techniques like LLM [51], [52] or MLLM [53] to further boost the new view synthesis performance, ultimately leading to improved CT reconstruction results.

## VI. CONCLUSION

We propose a dual view-guided diffusion model (DVG-Diffusion) to reconstruct CT from few view X-ray images, enhancing reconstruction quality through new-view synthesis and view-guided feature alignment. The proposed view parameter guided encoder (VPGE) facilitates the alignment

between 2D X-ray and 3D CT spaces. Additionally, using an auxiliary synthetic X-ray view and input X-ray views to jointly guide the latent diffusion model can reconstruct CT with better perceptual quality. This improvement is achieved through an efficient task decomposition, involving synthesizing new views, translating intricate 2D-to-3D mapping into a more feasible 3D-to-3D latent space mapping, and then reconstructing and refining CT volumes.

## REFERENCES

- [1] I. Sluimer, A. Schilham, M. Prokop, and B. Van Ginneken, "Computer analysis of computed tomography scans of the lung: a survey," *IEEE Trans. Med. Imaging*, vol. 25, no. 4, pp. 385–405, 2006.
- [2] D. Li, C. B. Patel, G. Xu, A. Iagaru, Z. Zhu, L. Zhang, and Z. Cheng, "Visualization of diagnostic and therapeutic targets in glioma with molecular imaging," *Front. Immunol.*, vol. 11, p. 592389, 2020.
- [3] Z. Chen, L. Guo, R. Zhang, Z. Fang, X. He, and J. Wang, "Bx2s-net: Learning to reconstruct 3d spinal structures from bi-planar x-ray images," *Comput. Biol. Med.*, vol. 154, p. 106615, 2023.
- [4] C.-M. Feng, B. Li, X. Xu, Y. Liu, H. Fu, and W. Zuo, "Learning federated visual prompt in null space for mri reconstruction," in *Proc. IEEE/CVF Conf. Comput. Vis. Pattern Recognit.*, pp. 8064–8073, 2023.
- [5] P. Guo, P. Wang, J. Zhou, S. Jiang, and V. M. Patel, "Multi-institutional collaborations for improving deep learning-based magnetic resonance image reconstruction using federated learning," in *Proc. IEEE/CVF Conf. Comput. Vis. Pattern Recognit.*, pp. 2423–2432, 2021.
- [6] Y. Jun, H. Shin, T. Eo, and D. Hwang, "Joint deep model-based mr image and coil sensitivity reconstruction network (joint-icnet) for fast mri," in *Proc. IEEE/CVF Conf. Comput. Vis. Pattern Recognit.*, pp. 5270–5279, 2021.
- [7] L. Qu, S. Wang, P.-T. Yap, and D. Shen, "Wavelet-based semi-supervised adversarial learning for synthesizing realistic 7t from 3t mri," in *Proc. Int. Conf. Med. Image Comput. Comput.-Assisted Intervention*, pp. 786–794, Springer, 2019.
- [8] L. Kong, C. Lian, D. Huang, Y. Hu, Q. Zhou, *et al.*, "Breaking the dilemma of medical image-to-image translation," *Adv. Neural Inf. Process. Syst.*, vol. 34, pp. 1964–1978, 2021.
- [9] L. Qu, Y. Zhang, S. Wang, P.-T. Yap, and D. Shen, "Synthesized 7t mri from 3t mri via deep learning in spatial and wavelet domains," *Med. Image Anal.*, vol. 62, p. 101663, 2020.
- [10] E. Hait and G. Gilboa, "Spectral total-variation local scale signatures for image manipulation and fusion," *IEEE Trans. Image Process.*, vol. 28, no. 2, pp. 880–895, 2018.
- [11] Y. Jiang, "Mfct-gan: multi-information network to reconstruct ct volumes for security screening," *J. Intell. Manuf. Spec. Equip.*, vol. 3, no. 1, pp. 17–30, 2022.
- [12] D. Kyung, K. Jo, J. Choo, J. Lee, and E. Choi, "Perspective projection-based 3d ct reconstruction from biplanar x-rays," in *2023 IEEE Int. Conf. Acoust. Speech Signal Process.*, pp. 1–5, IEEE, 2023.
- [13] X. Ying, H. Guo, K. Ma, J. Wu, Z. Weng, and Y. Zheng, "X2ct-gan: reconstructing ct from biplanar x-rays with generative adversarial networks," in *Proc. IEEE/CVF Conf. Comput. Vis. Pattern Recognit.*, pp. 10619–10628, 2019.
- [14] M. A. R. Ratul, K. Yuan, and W. Lee, "Ccx-raynet: a class conditioned convolutional neural network for biplanar x-rays to ct volume," in *IEEE 18th Int. Symp. Biomed. Imaging*, pp. 1655–1659, IEEE, 2021.
- [15] L. Shen, W. Zhao, and L. Xing, "Patient-specific reconstruction of volumetric computed tomography images from a single projection view via deep learning," *Nat. Biomed. Eng.*, vol. 3, no. 11, pp. 880–888, 2019.
- [16] A. Corona-Figueroa, J. Frawley, S. Bond-Taylor, S. Bethapudi, H. P. Shum, and C. G. Willcocks, "Mednerf: Medical neural radiance fields for reconstructing 3d-aware ct-projections from a single x-ray," in *Annu. Int. Conf. IEEE Eng. Med. Biol. Soc.*, pp. 3843–3848, IEEE, 2022.
- [17] R. Ge, Y. He, C. Xia, C. Xu, W. Sun, G. Yang, J. Li, Z. Wang, H. Yu, D. Zhang, *et al.*, "X-ctrsnet: 3d cervical vertebra ct reconstruction and segmentation directly from 2d x-ray images," *Knowledge-Based Syst.*, vol. 236, p. 107680, 2022.
- [18] S. Jecklin, C. Jancik, M. Farshad, P. Furnstahl, and H. Esfandiari, "X23d—*intraoperative 3d lumbar spine shape reconstruction based on sparse multi-view x-ray data*," *J. Imaging*, vol. 8, no. 10, p. 271, 2022.
- [19] Y. Wang, Z.-L. Sun, Z. Zeng, and K.-M. Lam, "Trct-gan: Ct reconstruction from biplane x-rays using transformer and generative adversarial networks," *Digit. Signal Prog.*, vol. 140, p. 104123, 2023.
- [20] P. Henzler, V. Rasche, T. Ropinski, and T. Ritschel, "Single-image tomography: 3d volumes from 2d cranial x-rays," in *Comput. Graph. Forum*, vol. 37, pp. 377–388, Wiley Online Library, 2018.
- [21] R. Hartley and A. Zisserman, *Multiple view geometry in computer vision*. Cambridge university press, 2003.
- [22] J. Ho, A. Jain, and P. Abbeel, "Denoising diffusion probabilistic models," *Adv. Neural Inf. Process. Syst.*, vol. 33, pp. 6840–6851, 2020.
- [23] O. Bar-Tal, H. Chefer, O. Tov, C. Herrmann, R. Paiss, S. Zada, A. Ephrat, J. Hur, Y. Li, T. Michaeli, *et al.*, "Lumiere: A space-time diffusion model for video generation," *arXiv preprint arXiv:2401.12945*, 2024.
- [24] X. Gao, Y. Yang, Y. Wu, S. Du, and G.-J. Qi, "Multi-condition latent diffusion network for scene-aware neural human motion prediction," *IEEE Trans. Image Process.*, 2024.
- [25] Y. Zhang, N. Huang, F. Tang, H. Huang, C. Ma, W. Dong, and C. Xu, "Inversion-based style transfer with diffusion models," in *Proc. IEEE/CVF Conf. Comput. Vis. Pattern Recognit.*, pp. 10146–10156, 2023.
- [26] Z. Ding, X. Zhang, Z. Xia, L. Jebe, Z. Tu, and X. Zhang, "Diffusionrig: Learning personalized priors for facial appearance editing," in *Proc. IEEE/CVF Conf. Comput. Vis. Pattern Recognit.*, pp. 12736–12746, 2023.
- [27] C.-Y. Chan, W.-C. Siu, Y.-H. Chan, and H. A. Chan, "Anlightendiff: Anchoring diffusion probabilistic model on low light image enhancement," *IEEE Trans. Image Process.*, 2024.
- [28] Z. Wang, B. Hu, M. Zhang, J. Li, L. Li, M. Gong, and X. Gao, "Diffusion model-based visual compensation guidance and visual difference analysis for no-reference image quality assessment," *IEEE Trans. Image Process.*, 2025.
- [29] T. Ancukėvičius, Z. Xu, M. Fisher, P. Henderson, H. Bilen, N. J. Mitra, and P. Guerrero, "Renderdiffusion: Image diffusion for 3d reconstruction, inpainting and generation," in *Proc. IEEE/CVF Conf. Comput. Vis. Pattern Recognit.*, pp. 12608–12618, 2023.
- [30] G. Qian, J. Mai, A. Hamdi, J. Ren, A. Siarohin, B. Li, H.-Y. Lee, I. Skorokhodov, P. Wonka, S. Tulyakov, *et al.*, "Magic123: One image to high-quality 3d object generation using both 2d and 3d diffusion priors," *arXiv preprint arXiv:2306.17843*, 2023.
- [31] X. Liu, S.-h. Kao, J. Chen, Y.-W. Tai, and C.-K. Tang, "Deceptive-nerf: Enhancing nerf reconstruction using pseudo-observations from diffusion models," *arXiv preprint arXiv:2305.15171*, 2023.
- [32] Y. C. Ahn, S. Jang, S. Park, J.-Y. Kim, and N. Kang, "Panerf: Pseudo-view augmentation for improved neural radiance fields based on few-shot inputs," *arXiv preprint arXiv:2211.12758*, 2022.
- [33] J. Gu, A. Trevisthick, K.-E. Lin, J. M. Susskind, C. Theobalt, L. Liu, and R. Ramamoorthi, "Nerfdiff: Single-image view synthesis with nerf-guided distillation from 3d-aware diffusion," in *Int. Conf. Mach. Learn.*, pp. 11808–11826, PMLR, 2023.
- [34] B. Poole, A. Jain, J. T. Barron, and B. Mildenhall, "Dreamfusion: Text-to-3d using 2d diffusion," *arXiv preprint arXiv:2209.14988*, 2022.
- [35] G. Metzger, E. Richardson, O. Patashnik, R. Giryes, and D. Cohen-Or, "Latent-nerf for shape-guided generation of 3d shapes and textures," in *Proc. IEEE/CVF Conf. Comput. Vis. Pattern Recognit.*, pp. 12663–12673, 2023.
- [36] A. Yu, V. Ye, M. Tancik, and A. Kanazawa, "pixelnerf: Neural radiance fields from one or few images," in *Proc. IEEE/CVF Conf. Comput. Vis. Pattern Recognit.*, pp. 4578–4587, 2021.
- [37] Y. Yao, Z. Luo, S. Li, T. Fang, and L. Qian, "Mvsnet: Depth inference for unstructured multi-view stereo," in *Proc. Eur. Conf. Comput. Vis.*, pp. 767–783, 2018.
- [38] A. K. Bhunia, S. Khan, H. Cholakkal, R. M. Anwer, J. Laaksonen, M. Shah, and F. S. Khan, "Person image synthesis via denoising diffusion model," in *Proc. IEEE/CVF Conf. Comput. Vis. Pattern Recognit.*, pp. 5968–5976, 2023.
- [39] H.-Y. Tseng, Q. Li, C. Kim, S. Alsisan, J.-B. Huang, and J. Kopf, "Consistent view synthesis with pose-guided diffusion models," in *Proc. IEEE/CVF Conf. Comput. Vis. Pattern Recognit.*, pp. 16773–16783, 2023.
- [40] B. Yang, S. Gu, B. Zhang, T. Zhang, X. Chen, X. Sun, D. Chen, and F. Wen, "Paint by example: Exemplar-based image editing with diffusion models," in *Proc. IEEE/CVF Conf. Comput. Vis. Pattern Recognit.*, pp. 18381–18391, 2023.
- [41] C. Peng, H. Liao, G. Wong, J. Luo, S. K. Zhou, and R. Chellappa, "Xraysyn: Realistic view synthesis from a single radiograph through ct priors," in *Proc. AAAI Conf. Artif. Intell.*, vol. 35, pp. 436–444, 2021.
- [42] P. Esser, R. Rombach, and B. Ommer, "Taming transformers for high-resolution image synthesis," in *Proc. IEEE/CVF Conf. Comput. Vis. Pattern Recognit.*, pp. 12873–12883, 2021.

- [43] F. Khader, G. Mueller-Franzes, S. T. Arasteh, T. Han, C. Haarburger, M. Schulze-Hagen, P. Schad, S. Engelhardt, B. Baessler, S. Foersch, *et al.*, “Medical diffusion–denoising diffusion probabilistic models for 3d medical image generation,” *arXiv preprint arXiv:2211.03364*, 2022.
- [44] S. G. Armato III, G. McLennan, L. Bidaut, M. F. McNitt-Gray, C. R. Meyer, A. P. Reeves, B. Zhao, D. R. Aberle, C. I. Henschke, E. A. Hoffman, *et al.*, “The lung image database consortium (lidc) and image database resource initiative (idri): a completed reference database of lung nodules on ct scans,” *Med. Phys.*, vol. 38, no. 2, pp. 915–931, 2011.
- [45] D. P. Kingma and J. Ba, “Adam: A method for stochastic optimization,” *arXiv preprint arXiv:1412.6980*, 2014.
- [46] C. Saharia, W. Chan, H. Chang, C. Lee, J. Ho, T. Salimans, D. Fleet, and M. Norouzi, “Palette: Image-to-image diffusion models,” in *ACM SIGGRAPH Conf. Proc.*, pp. 1–10, 2022.
- [47] R. Zhang, P. Isola, A. A. Efros, E. Shechtman, and O. Wang, “The unreasonable effectiveness of deep features as a perceptual metric,” in *Proc. IEEE/CVF Conf. Comput. Vis. Pattern Recognit.*, pp. 586–595, 2018.
- [48] H. Chung, D. Ryu, M. T. McCann, M. L. Klasky, and J. C. Ye, “Solving 3d inverse problems using pre-trained 2d diffusion models,” in *Proc. IEEE/CVF Conf. Comput. Vis. Pattern Recognit.*, pp. 22542–22551, 2023.
- [49] Z. Zhang, Q. Liu, and Y. Wang, “Road extraction by deep residual unet,” *IEEE Geosci. Remote Sens. Lett.*, vol. 15, no. 5, pp. 749–753, 2018.
- [50] A. E. Johnson, T. J. Pollard, N. R. Greenbaum, M. P. Lungren, C.-y. Deng, Y. Peng, Z. Lu, R. G. Mark, S. J. Berkowitz, and S. Horng, “Mimic-cxr-jpg, a large publicly available database of labeled chest radiographs,” *arXiv preprint arXiv:1901.07042*, 2019.
- [51] J. Achiam, S. Adler, S. Agarwal, L. Ahmad, I. Akkaya, F. L. Aleman, D. Almeida, J. Altschmidt, S. Altman, S. Anadkat, *et al.*, “Gpt-4 technical report,” *arXiv preprint arXiv:2303.08774*, 2023.
- [52] M. Song, J. Wang, Z. Yu, J. Wang, L. Yang, Y. Lu, B. Li, X. Wang, X. Wang, Q. Huang, *et al.*, “Pneumollm: Harnessing the power of large language model for pneumoconiosis diagnosis,” *Med. Image Anal.*, p. 103248, 2024.
- [53] C. Li, C. Wong, S. Zhang, N. Usuyama, H. Liu, J. Yang, T. Naumann, H. Poon, and J. Gao, “Llava-med: Training a large language-and-vision assistant for biomedicine in one day,” *Adv. Neural Inf. Process. Syst.*, vol. 36, 2024.